Meas. Sci. Technol. 5 (1994) 1480–1490. Printed in the UK

Direct and indirect dual-probe interferometers for accurate surface wave measurements

H P Ho, M G Somekh, M Liu and C W See

Department of Electrical and Electronic Engineering, University of Nottingham, University Park, Nottingham NG7 2RD, UK

Received 5 May 1994, accepted for publication 12 August 1994

Abstract. This paper describes the development and operation of two dual-probe interference systems for detection of surface acoustic waves. Both systems operate by comparing the surface displacement under each probe, thus enabling the surface wave velocity to be determined. In the so-called direct interference system the two probe beams are made to interfere with each other whereas in the indirect interference system each probe beam is made to interfere with a common reference. The relative merits of each system are compared in detail and experimental results showing operation of the systems are presented.

Nomenclature

A	Simplifying parameter $\eta\gamma\|E\|^2/(h\nu)$ (s^{-2})
B	Detection bandwidth of probe (Hz)
e	Electronic charge
E	Field strength of optical beam on emergence from source ($V\,m^{-1}$)
E_n	Field strength corresponding to the nth beam ($V\,m^{-1}$)
f_0	Optical frequency (Hz)
f	Drive frequency to Bragg cell (Hz)
f_s	Frequency of SAW wave (Hz)
h	Planck's constant (J s)
i	Photodetector current (A)
k_B	Boltzmann's constant ($J\,K^{-1}$)
k_s	Wavenumber of SAW wave $2\pi/\lambda_s$ (m^{-1})
k	Wavenumber of optical wave $2\pi/\lambda_{opt}$ (m^{-1})
m_{on}	Phase noise due to microphonics, n = probe number (1 or 2)
NA	Numerical aperture of probe optics
R	Photodetector load resistance (Ω)
$\boldsymbol{R}$	Amplitude reflection coefficient of interferometer reference beam
S_n	Amplitude reflection coefficient of the nth beam
T	Noise temperature of photodetector amplifier (K)
v_{ac}	Velocity of acoustic wave in Bragg cell ($m\,s^{-1}$)
v_s	SAW velocity ($m\,s^{-1}$)
Δv_s	Error in SAW velocity measurement ($m\,s^{-1}$)
x_n	Position of nth probe beam
α	Ratio of field strength of detected probe beam to laser output field strength
β	Ratio of field strength of common reference beam to laser output field strength
γ	Constant relating optical power to square optical field, power $=\gamma\|E\|^2$ ($m^2\,A^2\,s\,J^{-1}$)
$\delta(x)$	Instantaneous surface displacement as a function of position, x (m)
δ_0	Amplitude of surface displacement (m)
η	Quantum efficiency of photodetector
$\Delta\theta$	Angular separation of first-order and zeroth-order beams leaving the Bragg cell (rad)
λ_{opt}	Optical wavelength of probe beam (m)
λ_s	Wavelength of SAW (m)
ν	Optical frequency (Hz)
φ	Reference phase of SAW
$\Delta\varphi$	Phase error in SAW measurement of single probe (rad)
$\Delta\varphi_T$	Summed phase error in SAW measurement due to both probes (rad)
ψ	Phase of interference signal due to relative phase of reference and signal beams of interferometer
Δ	Extra optical phase difference between optical probes caused by surface topography (rad)

1. Introduction

One of the principal problems that beset ultrasonic non-destructive evaluation is the requirement to use contacting transducers. For many applications this disadvantage lies in the fact that access is often difficult with contacting probes. For some applications, such as the ones we are concerned with here, the main disadvantage of contacting probes is that they perturb the accuracy with which a particular measurement can be made. To overcome the problems involved in use of contacting probes, considerable effort has been made in development of optical techniques for generation and detection

0957-0233/94/121480+11 $19.50

of ultrasonic waves [1–6]. The disadvantage with these methods is that the efficiency of sound generation by thermal sources is rather low and similarly the sensitivity of ultrasonic detection with optical methods is poor compared with piezoelectric transducers.

Acoustic microscopy has been widely used in the so-called $V(z)$ mode [7, 8] for accurate determination of surface wave velocity. This technique involves scanning the axial separation between the lens and the sample, so producing an interference signal between the axially reflected wave and the surface wave excited on the sample surface. Determination of the periodicity of this interference pattern allows the surface wave velocity to be accurately determined. For many applications the main concern is not for absolute accuracy of measurement of the surface wave velocity but rather for detection of small changes in velocity. The sensitivity of the technique depends critically on the choice of acoustic lens, the precautions taken to maintain a constant fluid temperature and the precise nature of the signal processing technique used to extract the velocity measurements. It is reasonable to say that, in a conventional laboratory using commercial lenses, the changes in velocity that can be reliably measured correspond to approximately one part in 10^3, while sensitivities around an order of magnitude better can be achieved when the highest level of care is exercised [7]. There are several velocity measurement applications, such as film thickness measurement, assessment of surface damage, measurement of applied stress and determination of crystal orientation, which require, at least, the best sensitivity of which acoustic microscopy is capable [9–12].

The accuracy with which surface wave attenuation measurements can be performed in the acoustic microscope is even more severely limited by the requirement to use a coupling medium. The surface wave propagates along the solid/liquid interface, shedding energy continuously. The resulting measurement of attenuation is thus dominated by mode conversion back into the fluid rather than the intrinsic attenuation of the substrate. Clearly, therefore, non-contacting techniques are much better placed to perform accurate measurements of attenuation.

This paper discusses the development of two dual-beam optical interferometer systems for accurate measurement of surface wave velocity and attenuation. In this paper, we are particularly concerned with development of systems for probing continuous surface acoustic waves, although the techniques described here will, for the most part, be suited for probing SAW pulses also. The work described in this paper forms a portion of a larger project aimed at developing non-contacting generation and detection techniques for measuring small changes in surface wave velocity due to residual stress in the sample surface. In view of the remarks concerning the sensitivity of the techniques referred to in the first paragraph, considerable attention will be paid to the measures necessary to ensure that the system offers optimum performance in terms of signal-to-noise ratio and stability.

2. Interferometric detection of surface waves

The advantages of non-contacting detection of surface waves have long been recognized [13, 14], and accurate measurements of surface wave velocity have been carried out since the 1970s. Until recently, however, the interferometric systems have used one probe beam, which can detect the amplitude and phase of the SAW at a particular position. In order to measure the surface wave velocity with a single-probe system, it is necessary to move the sample mechanically. Dual-probe systems, which use two probe beams on the sample surface, have the advantage that sample scanning is not necessary because the separation time taken for the SAW to propagate between the beams can be used, thus obviating the need for mechanical displacement. One example of such is a system developed by Huang and Achenbach [15]. The probe beams, which are separated by 62.5 mm, form two arms of an interferometer, so that the relative displacement of the sample under each beam can be determined. This system, which produces the detection signal by direct interference between the two probe beams, is very effective for measuring the velocity over a distance long compared with the beam diameter. It is suitable for pulsed waveforms when the extent of the sound pulse is small relative to the separation of the beams. If the spacing is reduced too much, a true measurement of the surface displacement is not obtained, since both arms of the interferometer suffer displacement simultaneously. The systems described in the present paper are capable of measuring surface wave velocity and attenuation on a rather finer scale. Their designs are somewhat related to systems developed for profilometry and scanning optical microscopy [16] and thermal wave microscopy [17]. The direct system, which performs interference between the two probe beams, gives the surface wave velocity by noting the amplitude oscillation of the sideband when the probe separation is gradually changed. The indirect system uses the signals generated by making two probe beams interfere with a common reference arm. This configuration [18] gives two independent readings of surface displacement. Reliable measurements on velocity and attenuation can still be made when the surface wave is under both beams simultaneously. Furthermore, this not only has advantages in measurement of pulse waveforms but also enormously simplifies measurements of continuous wave surface waves. Development of the indirect configuration is a necessary step in measurement of surface wave velocity if recourse to beam scanning is to be avoided.

3. Optical configuration of direct and indirect dual-probe interferometers

3.1. The direct interference interferometer

Figure 1(*a*) shows the optical configuration of the direct interference interferometer used in this study, in many respects this system is similar to an earlier system

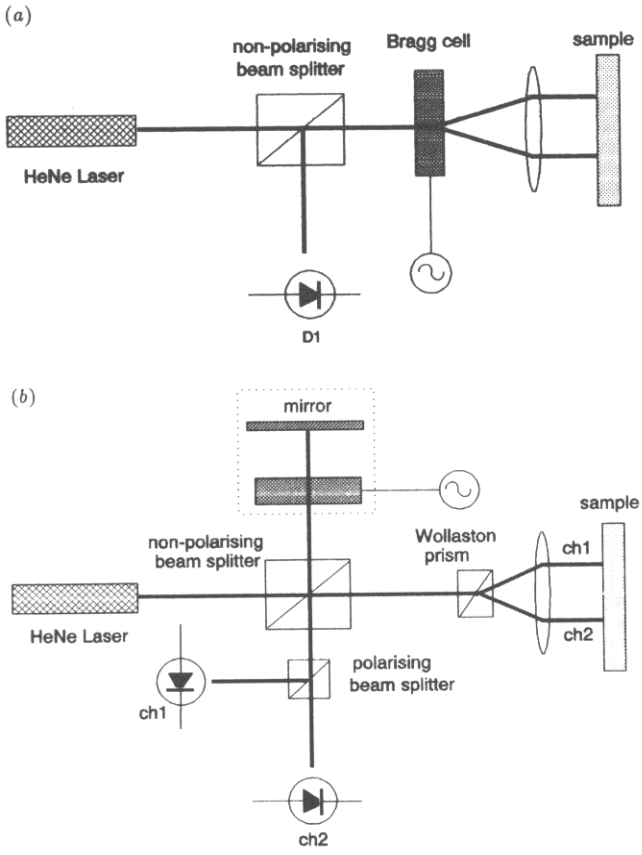

Figure 1. Dual-probe interferometers for the detection of surface waves: (*a*) direct configuration, (*b*) indirect configuration (the dashed box indicates incorporation of a reference beam, which distinguishes the system from a direct interferometer).

published by the authors for measurement of surface topography [16]. The output from the laser is directed to the sample through an acousto-optic (Bragg) cell, which splits the beam into zeroth-order and first-order components and also frequency-shifts the first-order diffracted beam by the drive frequency to the Bragg cell, f. The angular separation of the beams leaving the Bragg cell is given by

$$\Delta\theta = \sin^{-1}\left(\frac{f\lambda_{\mathrm{opt}}}{v_{\mathrm{ac}}}\right). \tag{1}$$

The objective lens whose back focal plane corresponds to the point at which the beams appear to split in the Bragg cell focuses these beams onto the sample at normal incidence. In practice, it is necessary to use relay optics both to expand the beams and to account for the fact that it is often not possible to place an objective sufficiently close to the Bragg cell. If relay optics are used, then the value of $\Delta\theta$ will be decreased by the same factor as the expansion of the beam diameter.

In the experiments reported here, the Bragg cell frequency was in the range 55–80.4 MHz, which corresponds to angular separation of 0.55°–0.80°.

When the beams are reflected from the sample surface they pass back through the Bragg cell, experiencing a second frequency shift. The interference signal is detected at the photodetector D1.

The output current at the photodetector is given by

$$i = \gamma(E_1 + E_2)(E_1 + E_2)^* \tag{2}$$

where E_1 and E_2 represent the fields at the detector corresponding to beams 1 and 2 respectively. If the initial field emerging from the laser is taken to be equal to E, then $E_1 = \alpha S_1 E \exp(\mathrm{j}2\pi f_0 t)$ and $E_2 = \alpha S_2 E \exp[\mathrm{j}2\pi(f_0 + 2f)t]$, where the factor α corresponds to the losses associated with lenses, Bragg cell, beamsplitters and other optical components, S_1 and S_2 are the amplitude reflection coefficients for beams 1 and 2 respectively and $\exp(\mathrm{j}4\pi f t)$ is the frequency shift imposed on beam 2 by double passage through the Bragg cell. The reflection coefficients for each beam have two components: the static sample-dependent reflection coefficient and a dynamically varying phase variation produced by periodic oscillation of the sample surface. The displacement, $\delta(x)$ of a surface acoustic wave (neglecting attenuation) is represented by

$$\delta(x) = \delta_0 \cos(2\pi f_s t - k_s x + \phi). \tag{3}$$

The photodetector output is given by

$$\begin{aligned}\frac{i}{A\alpha^2} &= |\boldsymbol{S}_1|^2 + |\boldsymbol{S}_2|^2 + 2|\boldsymbol{S}_1|\,|\boldsymbol{S}_2| \cos(4\pi f t + \psi) \\ &\quad - 2|\boldsymbol{S}_1|\,|\boldsymbol{S}_2| k\delta_0 \sin\left(\frac{k_s(x_2 - x_1)}{2}\right) \\ &\quad \times \cos\left(2\pi(2f + f_s)t + \varphi + \psi - \frac{k_s(x_2 + x_1)}{2}\right) \\ &\quad + 2|\boldsymbol{S}_1|\,|\boldsymbol{S}_2| k\delta_0 \sin\left(\frac{k_s(x_2 - x_1)}{2}\right) \\ &\quad \times \cos\left(2\pi(2f - f_s)t - \varphi + \psi + \frac{k_s(x_2 + x_1)}{2}\right).\end{aligned} \tag{4}$$

The assumption that $k\delta_0 \ll 1$ has been made and is clearly valid for the surface displacements likely to be encountered for continuous SAW (less than 1 nm). The four terms in the above equation are detected at different frequencies. The first and second terms are the DC terms corresponding to direct reflection from the sample surface. The third term is a carrier signal corresponding to the frequency shift imposed by the Bragg cell and the fourth and fifth terms are the upper and lower sidebands generated by surface vibration.

The amplitude of the third and fourth terms corresponding to the surface vibration in equation (3) varies sinusoidally with the probe separation (that is, phase difference of the SAW). It can be seen that, when the beam separation is an integer number of wavelengths, these terms vanish. Physically this arises from the fact that the sample under the two beams oscillates in phase, so that there is no relative displacement. Similarly the

relative displacement is a maximum when the beams are separated by an odd number of half SAW wavelengths. Furthermore, since the phase readings, $k_s(x_2+x_1)/2$, of these two terms only give the average of the absolute SAW phase under the probes but not the differential phase, they are difficult to separate from other phase contributions and are therefore not used for calculating the SAW velocity here.

3.2. The indirect interference interferometer

The indirect interference interferometer is shown in figure 1(*b*). In this system Bragg cells are also used but splitting of the two beams is performed by a Wollaston prism as shown. It should be emphasized, however, that the Bragg cell can be readily used as the splitting element in an indirect interferometer [18]. The crucial difference between the indirect interferometer and the direct interference system is the incorporation of the additional reference beam shown in the dashed box of figure (1*b*). This extra reference path greatly improves the flexibility of the system. It can be seen that beams 1 and 2 are no longer frequency-shifted with respect to each other, and do not interfere with each other because they have orthogonal polarizations. Each beam, however, interferes with the common reference path, whose polarization is adjusted so that it has a component parallel to each probe beam. The effect of this indirect configuration is that the system acts as two interferometers in parallel, which sense the oscillations of each beam.

The output from each channel of the interferometer is given by

$$\begin{aligned}\frac{i}{A} &= \alpha^2|\boldsymbol{S}_n|^2+\beta^2|\boldsymbol{R}|^2+2\alpha\beta|\boldsymbol{S}_n|\,|\boldsymbol{R}|\cos(4\pi ft+\psi)\\ &\quad+\alpha\beta|\boldsymbol{S}_n|\,|\boldsymbol{R}|k\delta_0\sin[2\pi(2f+f_s)t+\varphi+\psi-k_sx_n]\\ &\quad+\alpha\beta|\boldsymbol{S}_n|\,|\boldsymbol{R}|k\delta_0\sin[2\pi(2f-f_s)t-\varphi+\psi+k_sx_n].\end{aligned}\tag{5}$$

It can be readily seen that the indirect interferometer configuration gives two independent measures of the amplitude and phase of the SAW wave phase and can be applied equally to continuous wave or pulsed SAWs. The SAW velocity can be determined by comparing the phase of the carrier with the lower sideband for each channel, giving k_sx_n, and noting that the phase difference of the two channels is equal to $k_s(x_1-x_2)$; so, providing that the beam separation is known, the SAW velocity can be obtained.

3.3. The effect of microphonics and topography

Optical microphonics are variations of the phase output of the interferometer caused by vibration of optical components. In addition, the optical phase may also change according to variations in surface height and refractive index, which are associated with surface topography of the sample. All these effects can be taken into account by adding extra noise components to the equations derived in previous sections.

For the direct interferometer, we have

$$\begin{aligned}\frac{i}{A\alpha^2} &= |\boldsymbol{S}_1|^2+|\boldsymbol{S}_2|^2\\ &\quad+2|\boldsymbol{S}_1|\,|\boldsymbol{S}_2|\cos(4\pi ft+\psi+\Delta+m_{o2}-m_{o1})\\ &\quad-2|\boldsymbol{S}_1|\,|\boldsymbol{S}_2|k\delta_0\sin\left(\frac{k_s(x_2-x_1)}{2}\right)\\ &\quad\times\cos\left(2\pi(2f+f_s)t+\varphi+\psi+\Delta\right.\\ &\quad\left.-\frac{k_s(x_2+x_1)}{2}+m_{o2}-m_{o1}\right)\\ &\quad+2|\boldsymbol{S}_1|\,|\boldsymbol{S}_2|k\delta_0\sin\left(\frac{k_s(x_2-x_1)}{2}\right)\\ &\quad\times\cos\left(2\pi(2f-f_s)t-\varphi+\psi+\Delta\right.\\ &\quad\left.+\frac{k_s(x_2+x_1)}{2}+m_{o2}-m_{o1}\right).\end{aligned}\tag{6}$$

Clearly both the carrier and the sidebands are affected by microphonics. However, their overall effects, may cancel if $m_{o2}=m_{o1}$, which means that the contributions from microphonics are identical in both probes. Since the direct interferometer is largely common path except in the region where the beam is split into two probes and the separation between the probe is only a few SAW wavelengths, this condition will generally be satisfied.

For the indirect interferometer, we have

$$\begin{aligned}\frac{i}{A} &= \alpha^2|\boldsymbol{S}_n|^2+\beta^2|\boldsymbol{R}|^2\\ &\quad+2\alpha\beta|\boldsymbol{S}_n|\,|\boldsymbol{R}|\cos(4\pi ft+\psi+m_{on})\\ &\quad+\alpha\beta|\boldsymbol{S}_n|\,|\boldsymbol{R}|k\delta_0\\ &\quad\times\sin[2\pi(2f+f_s)t+\varphi+\psi-k_sx_n+m_{on}]\\ &\quad+\alpha\beta|\boldsymbol{S}_n|\,|\boldsymbol{R}|k\delta_0\\ &\quad\times\sin[2\pi(2f-f_s)t-\varphi+\psi+k_sx_n+m_{on}].\end{aligned}\tag{7}$$

Again we can see that the phase terms due to microphonics and topography exist in the carrier and the sidebands. It can be easily followed that microphonics will cancel if the SAW phase is calculated by comparing the phase measurements between the carrier and one of the two sidebands.

It should be mentioned that, for both systems, errors caused by frequency drifts in signal generators can be eliminated by using the same signal source for both generation and detection of the SAW signal.

3.4. Theoretical velocity measurement accuracy of SAW dual probe interferometers

The theoretical attainable measurement accuracy has been discussed in detail elsewhere [19] and this section will summarize the salient features. Emphasis will be given to the indirect interference system, which proves to be the most versatile system.

The fundamental noise mechanisms in an interferometer are the thermal noise and shot noise at the detectors. It can be shown that, provided that the signal power and the load impedance of the photodetector are sufficiently large, the shot noise dominates the thermal noise and the interferometer becomes shot-noise-limited. The shot noise is a white-noise source and will be present around the frequency of the sidebands, which carry the surface acoustic wave information. This introduces uncertainty in the measured phase of the sidebands, hence leading to a corresponding uncertainty with which the SAW velocity can be determined.

Assuming shot-noise-limited performance and that the size of the probe beam is negligible compared with the wavelength of the surface wave, it can be shown [19] that the uncertainty in measurement of the SAW phase by a single probe beam is given by

$$\Delta\varphi = \frac{i_{\text{noise}}}{\sqrt{2}i_{\text{signal}}} = \frac{1}{k_0\delta}\left(\frac{(\beta^2+4\alpha^2)Bh\nu}{\eta\gamma|E|^2\alpha^2\beta^2}\right)^{1/2} \qquad (8)$$

Since the phase uncertainties associated with the two probe beams are random and independent, the total error, $\Delta\varphi_T$, in measurement of the SAW phase is

$$\Delta\varphi_T = \sqrt{2}\,\Delta\varphi. \qquad (9)$$

Using optical powers of 1 mW from a He–Ne laser, $\alpha^2 = 0.1$, $\beta^2 = 0.05$, $\eta = 0.7$ and $B = 1$ Hz, this gives an overall phase uncertainty of $\pm 1.33 \times 10^{-3}$ rad for a surface displacement of 0.015 nm. The fractional velocity uncertainty is the ratio of the phase error divided by the phase shift in the propagation path between the two probe beams:

$$\frac{\Delta v_s}{v_s} = \frac{\Delta\varphi_T\,\lambda_s}{2\pi(x_1 - x_2)} \qquad (10)$$

where λ_s is the SAW wavelength. For a beam separation of ten SAW wavelengths, the minimum detectable SAW velocity variation for the conditions described above is approximately $\pm 0.002\%$ (or, an uncertainty of $\pm 0.00035\%$ for 30 s integration time). For larger surface displacements and optical powers, the performance increases accordingly. It should be noted that measurement uncertainty increases with the size of the probe beams relative to the wavelength of the surface wave. This will be further explained in later sections.

It is worth pointing out that the condition for shot noise to dominate the Johnson noise is that the load resistance R should satisfy the inequality

$$R \gg \frac{2k_B Th\nu}{\eta e^2(\beta^2+4\alpha^2)P}. \qquad (11)$$

For the values used earlier, this means that R should be approximately 10 kΩ or greater.

The analysis discussed above was for the indirect interference interferometer, for the direct system the analysis is a little more involved, depending on the exact beam separation and the measurement methodology employed. Suffice it to say for the present that, under optimum conditions, similar accuracy and sensitivity can be achieved with this configuration. The next section discusses some of the practical considerations that prevent theoretical accuracy being reached and some of the measures employed to approach this limit.

4. Practical implementation

In this section, we discuss development of the two interferometer systems for measuring surface wave velocity. More attention is paid to the indirect system, which has the best potential for accurate and above all simple measurements.

4.1. The direct interferometer

As depicted in figure 2, the optics required by a direct interferometer is straightforward. There are two main factors on which the relative SAW velocity measurement accuracy depends. These are (i) the number of SAW wavelengths (λ_s) covered by the probe separation and (ii) the signal-to-noise ratio of the sideband generated by the SAW. Factor (i) is primarily related to the size of the divergence angle ($\Delta\theta$) of the two beams and the focal length of the objective lens. Factor (ii) is related to the SAW amplitude, the laser power, the size of the probe relative to the SAW wavelength and the performance of the photodetector and subsequent detection electronics. In addition to the fundamental limitations on measurement accuracy, drift in the system will further limit the practical values that can be obtained. In practice, this is not much of a problem with the direct interferometer configuration but is more so with the indirect system, as will be described in the next section. This section discusses some aspects of interferometer operation in order to assess factors limiting measurement accuracy. The main purpose of this section is to enable comparison with the indirect interferometer, which is the most suitable system for continuous wave measurements.

In the current set-up the beam is expanded four times before entering the Bragg cell. The small value of $\Delta\theta$ available with the current Bragg cell means that the final focusing objective should have a long focal length in order to ensure that the probe separation covers a few surface acoustic wavelengths. This means that the spot size of the probes, which is determined by the effective numerical aperture of the objective, becomes large.

The low numerical aperture reduces the measurement sensitivity of the interferometer. This arises from the fact that high spatial frequencies of the surface wave are detected with less sensitivity. The phase modulation produced by a given displacement thus decreases as its wavelength becomes comparable to the focal spot size. The ideal situation occurs when the spot size is very small compared with λ_s. By considering the transfer function of a scanning microscope [21], it can be shown that the sensitivity becomes zero when $\lambda_{opt}/(2\text{NA}) = \lambda_s$. In our optical set-up, the constraints imposed by the present Bragg cell give a spot size of 24 μm (NA ≈ 0.03). The surface acoustic wavelength on lithium niobate at 100 MHz is approximately 39 μm, which, according to

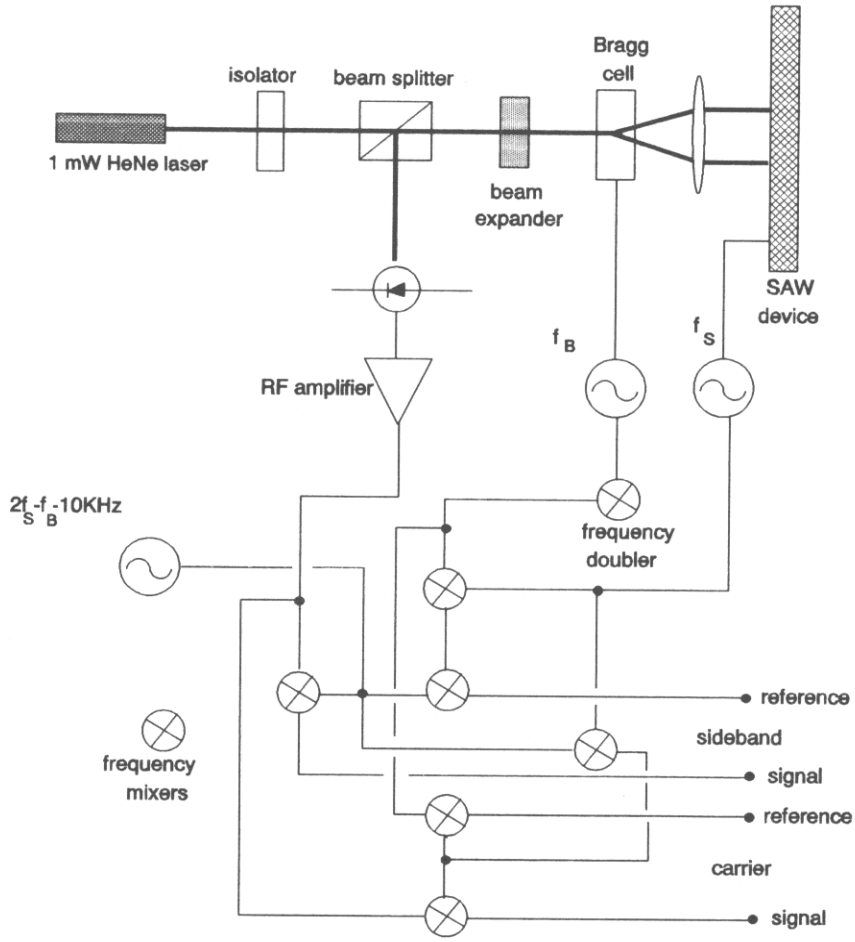

Figure 2. Direct interferometer and demodulation circuit for measuring surface wave velocity.

transfer function calculations and measurements by Suddendorf [20], leads to a reduction of sensitivity by a factor of 3.6.

In the present configuration the measurement sensitivity is also reduced by the detector. The front end of our photodetector consists of a high-frequency photodiode capacitor coupled to a high-frequency amplifier, which has an input impedance of 50 Ω. For our photodiode, which has a quantum efficiency of 0.7, the estimated optical input needed for shot noise to dominate Johnson noise is 24 mW. In our interferometer, the measured optical power reaching the photodetector is approximately 50 μW. The detection sensitivity is a long way from the shot-noise limit.

In addition to the above, it has been found that the Bragg cell is also responsible for some loss of sensitivity by introducing wavefront distortion to the laser beam. This is caused by the non-uniform field distribution of the acoustic bulk wave travelling inside the Bragg crystal. This is a problem with both direct and indirect configurations.

Clearly increasing the amplifier input impedance and increasing the optical power will improve the sensitivity of the system. In the particular implementation of the direct interference interferometer, the heterodyne frequency is varied from 110.0 to 160.8 MHz, which places a lower limit on the detection bandwidth, which prevents the use of high-input-impedance detection electronics. Similarly, the source power of the laser would need to be increased to approximately 500 mW, in order to increase the received detection power to the shot-noise limit. Since the emphasis of this paper is on the indirect interference system, these measures were not taken.

The effects described above mean that the displacement sensitivity of the direct beam interferometer in its present configuration is considerably poorer than the indirect beam system due to the need for high-frequency detectors; nevertheless, we will show in section 5 that the system can still be used for accurate measurement of surface wave velocity provided that the beams are scanned a sufficient distance.

4.2. The indirect interferometer

The system differs from the direct beam interferometer primarily by the incorporation of the extra reference beam, this means that the two probes form part of separate interferometers, which, as we have pointed out, makes the system most suitable for measurement of continuous surface waves. The probes can therefore be

kept at fixed positions in order to obtain the surface wave velocity measurements. Removal of the need to scan the probe beams obviously means that measurement time will be much shorter than that of the direct interferometer.

Practical implementation of the SAW measurement system is shown in figure 3, where considerable effort in optimizing component performance has been made in order to achieve high measurement sensitivity. For a 1 mW He–Ne source, the final optical power arriving at each of the four detectors is reduced to 10 μW due to the extra complexity of the indirect beam system. This means that great care must be exercised, especially when the system is operated with very low probe beam powers.

Another advantage of the indirect system is that the drive frequencies to the Bragg cell and the SAW device may be arranged in such a way that the lower sideband due to the SAW vibration occurs at low frequency so that shot-noise-limited detectors may be used. As shown in figure 3, there are two detectors for each channel. One detects the high-frequency carrier while the other detects the low-frequency sideband. A major drawback of the direct interferometer is that it has to use high-frequency amplifiers, which are not shot-noise-limited. This is not so much of a problem if only the carrier is detected since it has a very large signal-to-noise ratio. For detection of the sidebands, however, which are directly related to the SAW amplitude, it is important to make the amplifier shot-noise-limited. For this reason low-frequency detectors are used in our system to detect the lower sideband. The Bragg cell and SAW transducer drive frequencies have been chosen so that the lower sideband falls in a low frequency range (typically 1–30 kHz). For such frequencies low-noise operational amplifiers may be used

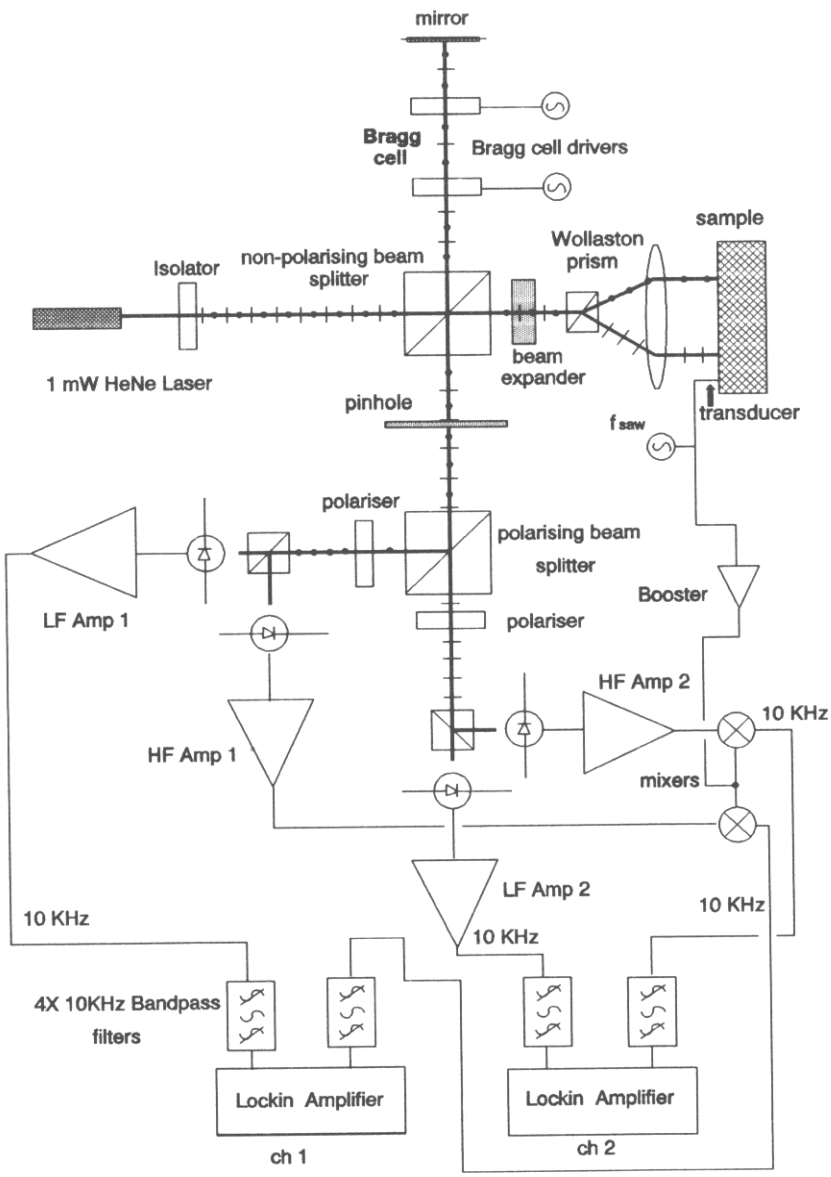

Figure 3. Indirect interferometer and demodulation circuit for measuring surface wave velocity.

to construct shot-noise-limited transimpedance amplifiers. Under these conditions there is virtually no restriction on the time constant of the amplifier and the load resistor may take large values (typically 100 kΩ). The detectors therefore give shot-noise-limited sensitivity, so that the limitation on the accuracy with which the surface wave phase can be measured arises from extrinsic factors whose effect and remedy are described in the next paragraph.

It has been found that the phase measurement varies slightly with ambient temperature. This is the major source of velocity measurement error in our experiments. It is believed that such error is caused by the combined effect between pointing variation of the laser beam due to relative movements of optical components and wavefront variation between the reference and signal beams due to distortion. Since each channel uses separate detectors to detect the carrier and the lower sideband, it is possible that the two detectors view slightly different parts of the beam and consequently experience slightly different phase drift. It has been found that such measurement drift may be reduced significantly by inserting a small pin-hole along the detection arm of the interferometer. The effect of the pin-hole is to limit the view of the detectors to a central region where the wavefront of the interfering beams should be nearly planar. Measurement error is therefore minimized, at the cost of reducing the power received by the detectors.

Furthermore, in order to minimize noise due to vibrations of optical components, low-profile components are used. The system is housed in an air-tight enclosure in order to ensure good isolation between the interferometer and the ambient environment.

Another source of measurement error that leads to drift arises from the back-reflected acoustic waves inside the diffracting medium of the Bragg cell. The effect is similar to that reported by Migdal *et al* [22], who developed a heterodyne system for measurement of optical absorption. In an ideal Bragg cell, all forward-travelling acoustic waves will be absorbed at the boundary of the crystal so that the optical beam is scattered by acoustic waves travelling in one direction. In practice, however, some of the acoustic waves will be back-reflected into the crystal. This means that some of the incident beam will be, for instance, up-converted by the forward-propagating wave in its first passage through the Bragg cell, and down-converted by the back-propagating wave in the second passage. Such a beam, which is not frequency-shifted, will emerge from the Bragg cell at precisely the same angle as the beam that is twice upshifted by the Bragg cell. These two beams interfere, giving a spurious signal at the carrier frequency whose phase drifts relative to true carrier signal. Our measured values of this spurious signal indicate that it can be as much as 25 dB below the actual carrier. The corresponding RMS phase error due to this spurious signal is $\pm 2.3°$. For a probe separation of $10\lambda_s$, this gives a velocity error of 0.15%. To reduce this effect we have incorporated a second Bragg cell along the reference arm (figure 3). This reduces the spurious signal by a further 25 dB since the only wave emerging from the two Bragg cells at the correct angle and the incorrect frequency must interact with the relatively weak back-reflected wave in both Bragg cells, which clearly has a much lower probability of occurrence than a single such interaction. The final error introduced by such an effect is less than $\pm 0.01°$. As will be discussed later, this is much smaller than that caused by other noise sources.

For the current set-up, the experimental detection sensitivity obtained from lithium niobate samples is 1.9×10^{-4} nm Hz$^{-1/2}$, which is four times inferior to the theoretical value of 4.8×10^{-5} nm Hz$^{-1/2}$ calculated assuming 10 μW optical power with the best case assumption of equal powers in the reference and signal beams. The effect of the finite size of the focal spots (in this case 15.6 μm) relative to the SAW wavelength (see section 4.1) is also included. The present experimental sensitivity value suggests that, in the current indirect system, the Bragg cell imposes less degradation in the SAW amplitude sensitivity than does the direct interferometer. This improvement is largely attributed to incorporation of the pin-hole, which cuts out the part of the laser beam where the wavefront is distorted; the remaining optical power arriving at the detectors will therefore produce a good interference signal. Incorporation of pin-holes also reduces the effects of thermal drift referred to later in this section.

In the experiments reported in the next section the surface amplitude and measurement time constant are respectively 0.015 nm and 30 s. Using the measurement sensitivity of 1.9×10^{-4} nm Hz$^{-1/2}$ the corresponding RMS phase measurement error is $\pm 0.09°$. This means that the $\pm 0.01°$ caused by the spurious carrier may be neglected. For a probe separation of $10\lambda_s$ this gives a SAW velocity measurement error of $\pm 0.0025\%$.

With adequate surface wave amplitudes, but without active temperature control, the most serious limitation in the present configuration appears to be drift introduced by variation in the ambient temperature. Figure 4 shows the variation of measured velocity against ambient temperature and the correlation is striking. The phase variation between the two beams, which corresponds to a velocity fluctuation of approximately 10 m s^{-1} K^{-1}, is about an order of magnitude larger than the actual change in velocity with temperature. To improve the repeatability of the system further, active temperature stabilization is thus required. We found that, without special precautions to limit the temperature variation, measurement drift over a period of 6 h was within $\pm 0.4°$. For the experiments described in the following section a probe separation of 1077 μm was used. With the SAW frequency at 37.44 MHz, the accuracy for silicon nitride ($\lambda_s = 154.7$ μm) will be limited to approximately three parts in 10^4. It should be mentioned that improvement is achieved if a larger number of surface wavelengths are contained inside the probe separation.

5. Measurement of SAW velocity with interferometer systems

This section demonstrates how the interferometer systems described previously may be used to make accurate

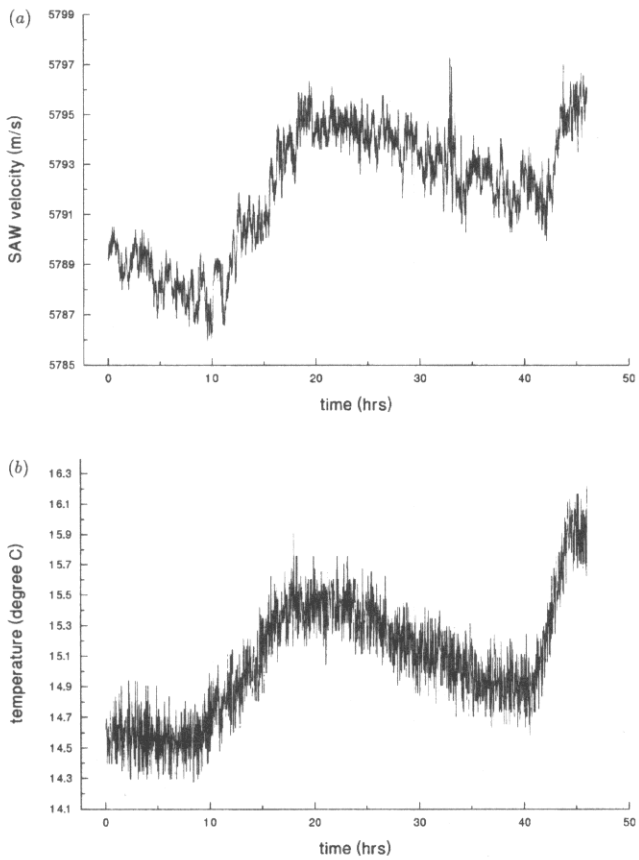

Figure 4. Plots of (*a*) measured surface wave velocity in silicon nitride and (*b*) temperature versus time to demonstrate the correlation between temperature and experimental error.

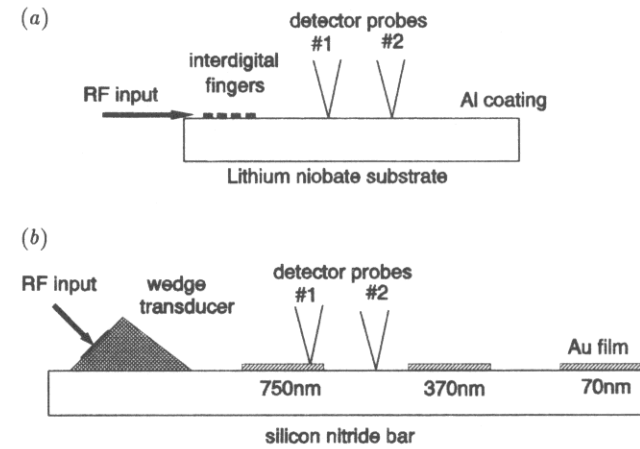

Figure 5. Schematics of samples: (*a*) surface wave device fabricated on lithium niobate, (*b*) surface wave excitation on silicon nitride by a wedge transducer.

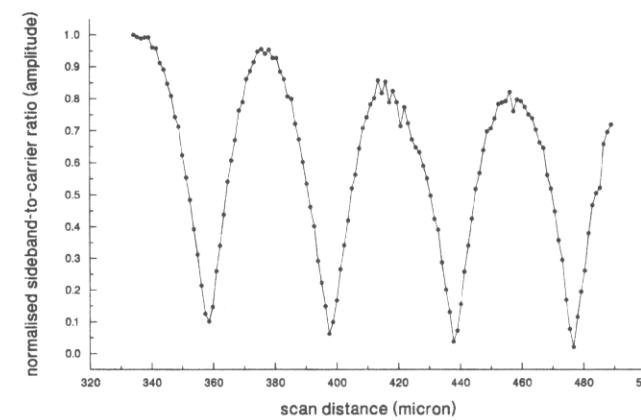

Figure 6. Plot of sideband-to-carrier ratio (amplitude) versus scan distance obtained from the direct interferometer. The sample is an un-coated lithium niobate surface wave device driven at 99 MHz.

measurements of surface wave velocity. Three sets of measurements have been performed to illustrate the effectiveness of the systems.

5.1. Direct and indirect SAW velocity measurements on $LiNbO_3$

The lithium niobate samples were 25 mm × 7 mm slices cleaved from a 41° *X*-rotated wafer. The surface waves were excited by a set of interdigital fingers (15 pairs) deposited on the sample (figure 5(*a*)). Measurements of the surface wave velocity were taken with both the direct and indirect systems so that a comparison between the two methods could be made.

The indirect interferometer measurements were performed by measuring the phase difference under each probe beam. The phase difference was then converted to a SAW velocity from knowledge of the beam separation and frequency. For direct interferometer measurements, the velocity was determined by noting the amplitude of the sideband generated from the interferometer when the drive frequency for the Bragg cell was scanned from 55 to 80.4 MHz in 128 steps. The separation of the probe beam thus varied from 334 to 489 μm. Figure 6 shows the interferometer response as a function of beam separation, where it can be seen to follow the oscillating form predicted by equation (4). The surface wave velocity was estimated from the periodicity of the dips in the curve. It is worth noting, in passing, that the data presented in figure 6 are amenable to Fourier analysis similar to that employed on the $V(z)$ curve [7, 12] in order to extract the most accurate estimate of SAW velocity.

The estimated surface wave velocity using the indirect interferometer was 3940 m s^{-1} at 100 MHz and 3935 m s^{-1} at 99 MHz with the direct interferometer. These results are in good agreement, particularly when we note that both methods are prone to *absolute* error due to uncertainty in the precise separations of the probe beams. Furthermore, the results obtained in the present experiments are comparable with published data [23].

5.2. Indirect interferometer measurement of coated silicon nitride

Since the main aim of the project is to measure small changes in surface wave velocity due to residual stress, we have performed an experiment on a silicon nitride bar, which was coated with gold layers of different

thicknesses. Perturbation of the surface by the surface layer will slightly reduce the surface wave velocity. Hence the performance of the system may be investigated. The silicon nitride samples were 50 mm × 5 mm × 3 mm bars with one of the 50 mm × 5 mm surfaces lapped. Surface waves of frequency 37.44 MHz were launched on the lapped surface using a conventional wedge transducer. The wedge, which was made from dense glass (SF6), had a width of 5 mm and the angle between the incident longitudinal wave generated from a lithium niobate transducer (3 mm wide) and the sample normal was 39.1°. This was the calculated critical angle for the glass/sample interface. Figure 5(*b*) shows the structure of the sample and where layers of gold of different thicknesses have been deposited. The layers are approximately 2 mm wide. The probes were scanned across the sample and the decrease in velocity relative to the bare substrate is plotted as a function of position in figure 7, curve A. Clearly, meaningful velocity measurements can only be obtained when both probes are incident above regions of similar coating thickness. The regions where valid measurements can be obtained are marked on curves B and C of figure 7, which show the variation in reflectivity as a function of position for the two beams. When both probes are used to examine similar regions, the reflectivities are similar, so that the reflectivity seen by each probe indicates where valid measurements may be taken. Figure 8 shows a plot of the experimentally determined surface wave velocity obtained by averaging the velocity values taken when both beams are incident on similar regions. The agreement between experimentally determined velocities and theoretical values can be seen to be good. The fluctuations in the results arise largely from the irregularity of coatings, which can be seen from the 'noise' on the reflectivity curves over the coated regions. Furthermore, back-scattered surface waves at the boundaries of the layers may also contribute to some of the fluctuations in the phase, and hence to the measured velocity, of the propagating surface wave.

5.3. Measurement of SAW velocity at different frequencies

The indirect interference interferometer has been used to compare the surface wave velocity at 37.44 and

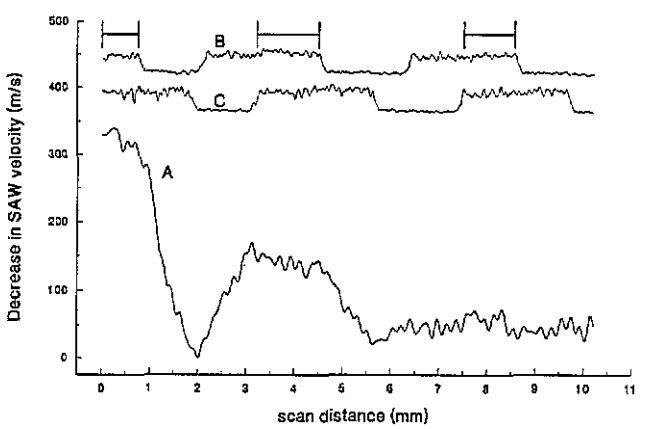

Figure 7. Plot of measured surface wave velocity reduction versus Au film thickness.

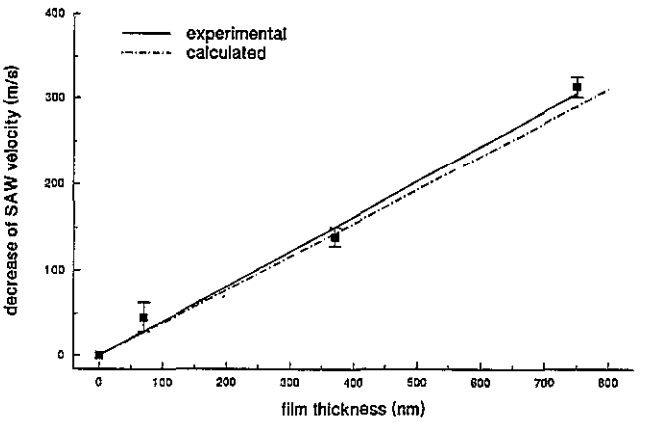

Figure 8. Comparison between experimental and calculated velocity reduction at different Au film thicknesses.

100.19 MHz. In both experiments the same wedge was used to launch the surface waves. For the high-frequency case the transducer was operated at its third overtone. Both experiments gave the same velocity measurement of 5787–5795 m s^{-1}. It should, however, be pointed out that the short-term measurement fluctuations in the two cases were different. At 37.44 MHz this was within ± 1 m s^{-1}, whereas at 100.19 MHz it was within ± 3 m s^{-1}. The larger fluctuation obtained at 100.19 MHz is primarily due to the fact that the SAW amplitude generated at this frequency is smaller by a factor of approximately eight times relative to the 37.44 MHz case.

These results indicate the essential trade-off inherent in measurements with this measurement system. Increase of the surface wave frequency means that the phase difference detected by the two beams of fixed separation will increase proportionately. This means that a given phase error results in a correspondingly smaller velocity error. On the other hand, the surface wave displacement and the effect of the optical transfer function mean that the measured displacement will generally be smaller at higher frequencies, with a corresponding increase in phase uncertainty. Naturally, the decision concerning the optimum operating frequency also depends on other factors such as the required depth penetration.

6. Conclusion

This paper has presented two dual-probe systems for accurate determination of changes in surface wave velocity. The direct system makes the two probes interfere directly and is similar to other systems developed for examination of pulsed acoustic waves. We describe a methodology for obtaining measurements on surface waves with this technique involving scanning the drive frequency to the acousto-optic device, which in turn scans a probe beam across the sample. The second system, the indirect interference interferometer, employs a common reference beam so that the system essentially consists of two interferometers in parallel. Analogous systems have been developed by the authors for examin-

ation of thermal waves but have not been used for determination of surface wave velocity, where we have shown it to be particularly suited for measurement of velocity and attenuation of continuous waves. In addition, the system has the additional advantage that surface wave measurements can be made rapidly without scanning either probe beam or using signal processing to extract the velocity value.

Considerable effort has been made to optimize the indirect interference system for accurate measurement of surface wave velocity and the measures to achieve this are described. We have calculated that the system should be capable of giving ideal shot-noise-limited performance and is capable of measuring the velocity of a SAW wave of amplitude 0.015 nm to an accuracy of 0.0012% using a probe separation of approximately seven wavelengths and a time constant of 30 s. However, despite using shot-noise-limited detectors the noise performance of the system was a factor of four worse than this, due primarily to wavefront distortion in the Bragg cells, thus giving a measurement error due to noise of approximately 0.005%. We have also shown that, without temperature control, limitation on sensitivity arises from instrumental drift due to temperature, which reduces the accuracy further to 0.03%.

Measurements have been performed on a range of samples demonstrating the capabilities of the system. The measurements on silicon nitride, which has an extremely high surface wave velocity, have also shown the importance of using a dual-probe system since it is difficult to obtain surface wave measurements with a high degree of accuracy using acoustic microscopy. The high velocity means that the periodicity of the $V(z)$ ripples is long so that very few cycles can be obtained on a typical curve, thus seriously reducing the measurement accuracy.

To conclude, we have presented two interferometer configurations capable of non-contacting measurement of surface wave velocity. The potential of the indirect interferometer, in particular, for even more accurate measurements is great. The system may be further improved if it is temperature-stabilized and a stable laser of considerably higher power is used. These changes will greatly reduce the drift and ensure that the detectors are shot-noise-limited respectively.

Acknowledgment

This work is supported by the European Commission under the Brite Euram project (contract number BE4398).

References

[1] Ash E A, Dieulesaint E and Rakouth H 1980 Generation of surface acoustic waves by means of CW laser *Electron. Lett.* **16** 470

[2] Telschow K L and Conent R J 1990 Optical and thermal parameter effects on laser generated ultrasound *J. Acoust. Soc. Am.* **88** 1494

[3] Karabutov A A 1985 Laser excitation of surface acoustic waves: a new direction in opto-acoustic spectroscopy of solid *Sov. Phys. – Usp.* **28** 1042

[4] Neubrand A and Hess P 1992 Laser generation and detection of surface acoustic waves: elastic properties of surface layers *J. Appl. Phys.* **71** 227

[5] Aharoni A, Tur M and Jassby M 1991 Monitoring material grain size by laser-generated ultrasound *Appl. Phys. Lett.* **59** 3530

[6] Davies S J, Edwards C, Taylor G S and Palmer S B 1993 Laser-generated ultrasound—its properties, mechanism and multifarious applications *J. Phys. D: Appl. Phys.* **26** 329

[7] Kushibiki J and Chubachi N 1985 Material characterisation by line-focus beam acoustic microscope *IEEE Trans. Sonics Ultrasonics* **32** 189

[8] da Fonseca P J M, Ferdi-Allah L, Despaux G, Boudour A, Robert L and Attal J 1993 Scanning acoustic microscopy—recent applications in material science *Adv. Mater.* **5** 508

[9] Meeks S W, Peter D, Horne D, Young K and Novotny V 1989 Microscopic imaging of residual stress using a phase-measuring acoustic microscope *Appl. Phys. Lett.* **55** 1835

[10] Stoodley N, Sklar Z, Scruby C and Briggs A 1994 Measurement of the effect of stress on the surface wave velocity of silicon using the line-focus beam acoustic microscope, to be published

[11] Weglein R D 1985 Acoustic micro-metrology *IEEE Trans. Sonics Ultrasonics* **32** 225

[12] Kushibiki J, Horii K and Chubachi N 1982 Leaky SAW velocity on water/silicon boundary measured by acoustic line-focus beam *Electron. Lett.* **18** 732

[13] Whitman R L and Korpel A 1969 Probing of acoustic surface perturbations by coherent light *Appl. Opt.* **8** 1567

[14] De La Rue R M, Humphryes R F, Mason I M and Ash E A 1972 Acoustic-surface-wave amplitude and phase measurement using laser probes *Proc. IEE* **119** 117

[15] Huang J and Achenbach J D 1991 Dual-probe laser interferometer *J. Acoust. Soc. Am.* **90** 1269

[16] See C W, Appel R K and Somekh M G 1988 Scanning differential profilometer for simultaneous measurement of amplitude and phase variation *Appl. Phys. Lett.* **53** 10

[17] Suddendorf M B, Liu M and Somekh M G 1992 A new high-resolution dual probe system for detection and imaging thermal and plasma waves *Scanning* **14** 247

[18] Valera M S, Somekh M G and Appel R K 1991 Common path differential intensity and phase profilometer using time division multiplexing *Electron. Lett.* **27** 719

[19] Jiang Z L and Somekh M G 1992 Analysis of surface acoustic wave measurement accuracy using interferometric detection *14th Int. Conf. on Acoustics, Beijing* pp A13–9

[20] Suddendorf M B 1994 Laser scanning probes for thermal wave material characterisation and microscopy *PhD Thesis* University of Nottingham

[21] Wilson T and Sheppard C 1984 Theory and practice of scanning microscopy (London: Academic) p 51

[22] Migdal A L, Roop B, Zheng Y C, Hardis J E and Xia G J 1990 Use of heterodyne detection to measure optical transmittance over a wide range *Appl. Opt.* **29** 5136

[23] Hinkov V 1989 Velocity of SAWs on lithium niobate: anisotropy, temperature and composition dependence *Properties of Lithium Niobate* (London: INSPEC, IEE) p 94